Spatio-temporal patterns in methane flux and gas transfer velocity at low wind speeds:

Implications for upscaling studies on small lakes

J. Schilder[1,2], D. Bastviken[3], M. van Hardenbroek[1,4], and O. Heiri[1]

[1]Institute of Plant Sciences and Oeschger Centre for Climate Change Research, University of Bern, Altenbergrain 21, 3013 Bern, Switzerland.

[2]Department of Biological and Environmental Science, University of Jyväskylä, PO Box 35, 40014 Jyväskylä, Finland*

[3]Department of Thematic Studies-Water and Environmental Studies, Linköping University, Linköping 581 83, Sweden.

[4]Geography and Environment, University of Southampton, Southampton SO17 1BJ, United Kingdom.

Corresponding author: Jos Schilder (j.c.schilder@gmail.com)

*Current address

Key Points:

- Wind-speed dependency of gas transfer velocity was investigated on a small lake over 14-months
- Diffusive and ebullitive methane fluxes showed strong temporal and within-lake spatial variability
- Accounting for spatio-temporal variability can improve aquatic greenhouse gas emission estimates

This article has been accepted for publication and undergone full peer review but has not been through the copyediting, typesetting, pagination and proofreading process which may lead to differences between this version and the Version of Record. Please cite this article as doi: 10.1002/2016JG003346

Abstract

Lakes contribute significantly to the global natural emissions of methane (CH_4) and carbon dioxide. However, to accurately incorporate them into the continental carbon balance more detailed surveys of lacustrine greenhouse gas emissions are needed, especially in respect to spatio-temporal variability and to how this affects the upscaling of results. We investigated CH_4 flux from a small, wind shielded lake during 10 field trips over a 14-month period. We show that floating chambers may be used to calibrate the relationship between gas transfer velocity (k) and wind speed at 10 m height (U_{10}) to the local system, in order to obtain more accurate estimates of diffusive CH_4 flux than by applying general models predicting k based on U_{10}. We confirm earlier studies indicating strong within-lake spatial variation in this relationship, and in ebullitive CH_4 flux within the lake basin. However, in contrast to the pattern reported in other studies, ebullitive CH_4 flux was highest in the central parts of the lake. Our results indicate positive relationships between k and U_{10} at very low U_{10} (0 – 3 m s^{-1}), which disagrees with earlier suggestions that this relationship may be negligible at low U_{10} values. We estimate annually averaged open water CH_4 emission from Lake Gerzensee to be 3.6 - 5.8 mmol m^{-2} day^{-1}. Our data suggest that estimates of greenhouse gas emissions from aquatic systems to the atmosphere based on the upscaling of short-term and small-scale measurements can be improved if both spatial and temporal variability of emissions are taken into account.

1 Introduction

Lakes, rivers and wetlands are a major source of carbon dioxide (CO_2) and methane (CH_4) to the atmosphere [*Bastviken et al*., 2004; *Cole et al*., 2007; *Tranvik et al*., 2009]. The amount of these potent well-mixed greenhouse gases [*Myhre et al*., 2013] emitted by freshwater bodies has been argued to offset part of the carbon sink capacity of the terrestrial realm [*Cole et al*., 2007; *Bastviken et al*., 2011]. Therefore, the inclusion of freshwater bodies in the global greenhouse gas balance has been called for [*Cole et al*., 2007; *Battin et al*., 2009; *Bastviken et al*., 2011]. Lakes form an important part of the terrestrial freshwater bodies [*Downing and Duarte*, 2009]. The number of field studies measuring greenhouse gas emissions from lakes is limited, however, and often such measurements are representative of only a section of the examined lakes and performed during a short time of the year. Only few studies are available which document variations in greenhouse gas emissions of individual lakes over an entire seasonal cycle [e.g *Miettinen et al*., 2015; *Wik et al*., 2016]. As a consequence, upscaled estimates of global greenhouse gas emissions from lakes are largely based on short-term, small-scale measurements [*Bastviken et al*., 2011]. Similarly, the spatial variability of gas flux across lake basins, and the effects of variables such as lake morphology and wind direction on these spatial patterns have received relatively little attention in previous studies [*Schilder et al*., 2013; *Vachon and Prairie*, 2013; *Wik et al*., 2016]. Improving our understanding of temporal and spatial variability in fluxes of greenhouse gases from lakes is therefore essential for upscaling field measurements, and for the incorporation of freshwater systems into the terrestrial greenhouse gas balance.

Up to 50 % of the open water CH_4 emissions by lakes occurs via diffusive flux (F) at the air-water interface [*Bastviken et al*., 2004], while F is the main mode of emission for the more soluble CO_2 [*Bade*, 2009]. Gas bubbles formed in and released from the sediment (ebullition, E) is the other main pathway of open water CH_4 flux from lakes [*Bastviken et al*., 2004]. A widely used method to quantify F from lakes is to estimate F from the lake surface

based on wind speed and surface water concentrations of the gas of interest by applying the following equation:

(1) $F = k(C_{aq} - C_{eq})$

where F is diffusive flux (mmol m^{-2} day^{-1}), C_{aq} is the surface water concentration (mmol m^{-3}), C_{eq} is the theoretical surface water concentration of the gas in equilibrium with the air (calculated following Henry's Law), and k is the gas exchange coefficient (m d^{-1}). Empirical relationships between wind speed at 10 m height (U_{10}) and gas transfer velocity are frequently used to estimate k. There are a number of datasets available to model k based on wind speed [e.g. *Liss and Merlivat*, 1986; *Cole and Caraco*, 1998; *Crusius and Wanninkhof*, 2003], typically based on tracer gas experiments using SF_6. Several studies have pointed out, however, that the choice of one model alone can cause F estimates to differ from 50 – 200 % between models [e.g. *Cole et al*., 2010; *Schubert et al*., 2012; *Schilder et al*., 2013]. Furthermore, there are major differences in the relationship between U_{10} and k at low wind speeds between these models. Some models indicate no relationship at low wind speeds [e.g. *Crusius and Wanninkhof*, 2003] (model C in their Figure 3), others a linear relationship, but with slopes varying between models (0.17 to 0.72; e.g. [*Crusius and Wanninkhof*, 2003], model A in their Figure 3; [*Liss and Merlivat*, 1986]), while *Cole and Caraco* [1998] propose an exponential relationship. It remains unclear to what extent these general models can be applied to lake types not included in the calibration data, and whether they are able to successfully predict varying k and F at low wind speeds. The case has been made that the relation between U_{10} and k is best calibrated to the local system [*Schilder et al*., 2013; *Vachon and Prairie*, 2013] and that floating chambers, if properly designed, can be used to do so, using diffusive CH_4 flux to infer k [*Cole et al*., 2010; *Gålfalk et al*., 2013; *Schilder et al*.,

2013]. Recent studies have shown that lake morphology and within-lake spatial heterogeneity in C_{aq} and k may be causes for discrepancies between models that predict k based on U_{10} [*Read et al*., 2012; *Schilder et al*., 2013; *Vachon and Prairie*, 2013]. These studies suggest an effect of lake size and shape on the relationship between k and U_{10}, and that the strength of this effect is related to the distance to shoreline.

E has been found to be highly variable on both temporal and spatial scales, due to e.g. variation in sediment composition, impact of wave action and sensitivity to atmospheric pressure changes [*Keller and Stallard*, 1994; *Mattson and Likens*, 1990; *Hofmann et al*., 2010; *Wik et al*., 2011]. Most studies (mostly focused on tropical and boreal systems) report higher E in areas closer to shore and macrophytes and note that in order to representatively capture E with floating chambers, measurement series encompassing more than 24 hours are needed to account for the strong temporal variability in E [e.g. Bastviken et al., 2004; Peixoto et al. 2015].

In this study we examine the relationship between U_{10} and k for Lake Gerzensee, a small (0.24 km^2) dimictic lake in Switzerland with exceptionally high CH_4 concentrations in the surface water and hypolimnion [*Rinta et al*., 2015]. To develop site-specific relationships between k and U_{10}, and to explore the spatial heterogeneity in F and k proposed by *Schilder et al*. [2013] and *Vachon and Prairie* [2013] we made detailed assessments of k for 10 different locations along three spatial transects on the lake during four 48-h sampling campaigns in October and November 2012 and March and June 2013, along with wind speed measurements (Table 1). These site-specific relationships between k and U_{10} were then used to derive a whole-lake relationship between k and U_{10}, which was applied to infer whole-lake F estimates based on C_{aq} and U_{10} measured during 10 lake visits between October 2012 and December 2013, including the four campaigns mentioned above, which allowed us to investigate temporal variability in F from the lake. Additionally, we estimated E along these

spatial transects on 6 occasions between October 2012 and September 2013 in order to assess the relative importance of both (*E* and *F*) open water CH_4 flux pathways and to investigate within-lake spatial patterns in *E* in Lake Gerzensee. Our aims included to describe variations in *E* and *F* of CH_4 across an annual cycle, provide an estimate of the overall CH_4 flux from the lake, and examine the extent to which a locally calibrated relationship between *k* and U_{10} based on a limited number of floating chamber measurements can improve estimates of *F* based on C_{aq} and U_{10}-derived *k*. Finally, since high wind speeds are relatively rare at Lake Gerzensee due the surrounding landscape features, we could investigate the relationship between U_{10} and *k* at very low wind speeds, on which existing models do not agree well.

2 Materials and Methods

Lake Gerzensee was sampled on 10 1 to 3-day visits between October 2012 and December 2013 to measure spatial variations in *k* (4 visits), spatial variations in total CH_4 flux and *E* (sampling at the above 4 visits plus 2 extra visits) and CH_4 concentrations in surface water to allow estimates of *F* based on the locally established relationship between U_{10} and *k* (10 visits, including the abovementioned 6). The sampling campaign is summarized in Table 1.

2.1 Floating chambers

CH_4 accumulation was measured in floating chambers following the design by *Cole et al*. [2010]. These chambers provide *F* and *k* estimates that are comparable to other methods [*Cole et al*., 2010; *Gålfalk et al*., 2013; *Schilder et al*., 2013]. The main disadvantage of the method is that *E* may be captured in the chambers. *Bastviken et al*. [2004] have shown that there are simple numerical procedures to identify chambers that have received *E*. However, on lakes with a high probability of *E* the chamber design has to be modified to obtain proper estimates of *F* and *k*. Therefore, some chambers were adapted following *Bastviken et al*.

[2010] by suspending plastic shields (Avento Snow Disc) with twice the diameter of the chamber under the floating chambers using 2 mm thick steel wires (Figure 1a,b). While the shields used by *Bastviken et al*. [2010] were aimed at deflecting rising gas bubbles, our shields were slightly concave and captured the bubbles. 100 g weights were attached to the top of the shields to reduce their buoyancy and ensure that they remain suspended below the floating chambers.

2.2 Field campaign design

2.2.1 Spatial variation in *k*

In order to obtain a lake-specific relationship between U_{10} and *k*, Lake Gerzensee was visited on 1-3 October and 26-28 November 2012, and 26-28 March and 10-12 June 2013 for 48 h of consecutive determinations of *k* (see below) along three spatial transects from lake shore (just beyond emerging macrophytes) to centre. Each transect consisted of four sampling sites represented by a floating chamber with ebullition shield, and all transects shared the same central floating chamber (locality D, Figure 1c). A handheld GPS device (Garmin, USA), an echosounder (Uwitec, Austria) and landmarks were used to ensure the chambers were on the same location during each lake visit. Wind speed (m s^{-1}) and absolute air pressure (hPa) were recorded on the northern shore using a portable weather station (Velleman, Belgium) at a height of 2.5 m (Figure 1). Wind speed was measured at 5 minute intervals and then averaged for the deployment period for each chamber. During these 48 h, CH_4 accumulation in the shielded chamber headspace was determined after 6 h (ca. 10:00 to 16:00) and after 24 h (ca. 10:00 to 10:00 the next day). After 24 h the chambers were lifted from the water, equilibrated with ambient air and re-deployed. The chamber headspace was sampled again after three

further 2 h intervals (at ca. 12:00, 14:00 and 16:00) and after 24 h (ca. 10:00 on day 3). This routine potentially yielded 60 estimates of *F* per lake visit, divided amongst ten sampling stations: Each station yielded three 2 h measurements, two 18 h measurement and one 6 h measurement. Due to a technical malfunction during the first night of the March 2013 excursion the first 18 h *F* measurements did not have accompanying wind speed measurements and due to time constraints we limited the June excursion to two sets of 24 h *F* measurements, with no intermediate measurements. As a consequence, the total number of *F* determinations per sampling station was 19 during the first four 3-day visits, yielding a total of 190 measurements. At each sampling station, a sample for determining C_{aq} was taken as described below at the start of day one and every time the floating chamber headspace was sampled. C_{eq} and measurements of *F* and C_{aq} were used to infer estimates of *k* following equation (1). Wind speed was converted to U_{10} following *Bade* [2009] using the equation:

(2) $$U_{10} = 2.5\left[1 + \frac{(C_d)^{0.5}}{\kappa} ln\left(\frac{10}{2.5}\right)\right]$$

in which C_d is the drag coefficient at a height of 10 m ($1.3 \cdot 10^{-3}$) and κ the Van Karman constant
(0.4, [*Bade*, 2009]).

2.2.2 Spatial variation in *E*

In order to investigate and quantify spatial variability in *E* from Lake Gerzensee, floating chambers without ebullition shield were deployed along the transects on 1-3 October and 26-28 November 2012, and on 26-28 March, 10-12 June, 29-31 July, and 23-25 September 2013 (Table 1; Figure 1c). One chamber was deployed at each locality, except for locality D, which had three chambers. The chambers were deployed for 24 h, after which the chamber

headspace was sampled and the chambers were lifted from the water and equilibrated with ambient air. Then, after another 24 h, the chamber headspace was sampled again and the average of two consecutive 24 h measurements was calculated in order to account for temporal variability in *E*. At each sampling station, a sample for determining C_{aq} was taken as described below at the start of day one and every time the floating chamber headspace was sampled. CH_4 accumulation in the unshielded chambers was used as an indication of total open water CH_4 flux ($E + F$), and F, based on C_{aq}, U_{10} and our locally calibrated relationships between U_{10} and k, was subtracted from total CH_4 flux to obtain an estimate of E.

2.2.3 Upscaling to the whole-lake level

A digital map of Lake Gerzensee and the sampling stations was created using ArcGIS (Esri). Then, Thiessen polygons were generated which identified the closest sampling station for each point on the lake. These polygons were used to estimate the proportion of the lake represented by the different chamber locations (see Table 2). To the sampling stations closest to the shore (A1, B1 and C1) a 10 m wide strip of lake area tracing the shoreline was assigned. The proportion of the lake represented by each sampling station was used to derive whole-lake estimates by multiplying the value for a variable at each sampling station with the proportion of lake it represented and adding up the results for all sampling stations.

2.3 Gas sampling and analysis

Samples from the floating chamber headspace were taken by withdrawing 30 ml of the gas with a 60 ml syringe (Becton-Dickinson, USA) equipped with a stopcock. 20 ml of the gas was then injected into a 12 ml glass vial with septum (Labco, UK) filled with a saturated brine solution, using a second needle to allow some of the brine to escape. The brine solution prevents dissolution and oxidation of CH_4 in the sample headspace [*Bastviken et al*., 2010].

All samples taken during this study were stored in the dark and upside-down between sampling and measuring, to ensure that gas could not exchange through the septum.

During the first six 3-day visits, C_{aq} was determined at each sampling station by sampling 40 ml water from 10 cm below the water surface and 20 ml of ambient air with a 60 ml syringe equipped with a stopcock. The water and air trapped in the syringe were allowed to equilibrate by shaking for 60 s. The 20 ml of headspace from the syringe were then injected into a 12 ml glass vial as described above. C_{aq} was determined at the beginning of day 1 and each time floating chamber headspaces were sampled. Simultaneously with sampling surface water for C_{aq}, we recorded surface water temperature (WTW LF 330, TetraCon© probe, Germany) and sampled 20 ml of ambient air into 12 ml vials as described above. These samples were used to determine the CH_4 concentration of the air the C_{aq} samples were equilibrated with and to determine initial in-chamber CH_4 concentrations. During each of the 4 shorter visits between October and December 2013, three samples of ambient air and C_{aq} in the lake centre (stadion D) were taken as described above. Within six weeks of sampling, the CH_4 concentrations in the samples were determined through gas chromatography using a flame ionization detector equipped with a methanizer (Shimadzu GC-2014, ShinCarbon ST column). C_{aq} was calculated following *Bastviken et al*. [2010].

2.4 Estimating *k*

The CH_4 accumulation in the shielded floating chamber headspace gives, when accounting for chamber area, volume and deployment duration, an estimate of F. Since C_{aq} was measured and

C_{eq} can be calculated (using Henry's Law), equation 1 can be used to infer *k*. However, since the concentration gradient (C_{aq}-C_{eq}) decreases with increasing CH_4 concentrations in the chamber headspace, *F* into the floating chamber headspace is not linear over time. Therefore, *k* was corrected for this changing concentration gradient using the method described by *Cole et al.* [2010]. In order to allow for comparison with other studies involving *k*, these corrected *k* values were then converted to k_{600}, the *k* value for CO_2 at 20° C following *Bade* [2009]. These k_{600} values were then converted from m day^{-1} to cm h^{-1}, the unit commonly used to report k_{600} values in literature.

On 14 and 30 October and 14 November 2013, three replicate shielded chambers were deployed at the same station (D) for 2 h, to obtain an indication of the reproducibility of our shielded floating chamber k_{600} estimates. The standard deviation of the 3 replicate k_{600} estimates on 14 and 30 October and 14 November 2013 was 0.2, 0.05 and 0.1 cm h^{-1}, respectively (coefficient of variation 12, 4 and 8 %, respectively).

2.5 Whole-lake *F* estimates based on U_{10}-inferred *k*-values

Our estimates of U_{10} and of the accompanying *k* for each sampling site during the first 6 visits allowed for the construction of sampling site-specific relationships between U_{10} and *k*. Whole-lake *F* estimates from Lake Gerzensee were then calculated based on the whole-lake relationship between U_{10} and flux chamber derived k_{CH4} (calculated as the area weighted average of estimates inferred from the sampling site-specific relationships as outlined in section 2.2.3), and whole-lake C_{aq} obtained through measurements at each chamber. Since average whole-lake C_{aq} was not significantly different from C_{aq} at sampling site D in the lake centre during the first 6 visits (see Results and Discussion), four further estimates of whole-lake *F* were made based on C_{aq} at sampling station D only and U_{10}-derived estimates of whole-lake k_{CH4}: On 14 and 30 October, 14 November, and 2 December 2013 three replicate

samples for C_{aq} were taken at sampling station D. $U_{2.5}$ was monitored on the northern shore between ca. 08.00 and 12.00 during these 4 additional lake visits. On 14 October 2013 we were unable to measure $U_{2.5}$ due to technical difficulties and obtained wind speed data from the Swiss national weather service (Meteo Swiss, Zurich) measured in Thun, 9 km from the lake.

2.6 Statistical analyses

All statistical analyses were performed with the PAST software package, version 1.97 [*Hammer et al.*, 2001]. Linear regressions and Pearson´s correlations were used to test the relationships between U_{10} and k_{600} for the sampling sites and a paired t-test was applied to test for differences between whole-lake C_{aq} and C_{aq} at the central sampling site.

3 Results and discussion

3.1 Data screening

All measurements from the shielded chambers with potential influence of E or chamber leakage were rejected. For example, for twenty of the seventy 18 h F measurements we noticed that gas accumulation under the shield had caused the shield to tilt and to no longer fully shield the chamber. Five additional measurements were eliminated because they yielded k_{600} values distinctly (3 to 10 times) higher than other measurements at that sampling station during that specific visit, suggesting E contributed to gas concentrations in the chamber headspace [*Bastviken et al.*, 2004], and one sample was lost during sampling. Finally, six k_{600} estimates were eliminated from further analyses since unrealistically low k_{600} values (between 0.2 and 0.5 cm h^{-1}) compared to other measurements, as well as in comparison with k_{600}

values in the literature, suggested chamber leakage. This data screening reduced our data set from 190 to 158 data points divided over 10 sampling stations.

3.2 Relationships between U_{10} and k_{600}

U_{10} was low during all measurements (between 0.05 and 2.67 m s^{-1}), and throughout the visits there was one dominant wind direction (Northeasterly). The accompanying k_{600} values were between 0.62 and 5.57 cm h^{-1}. Vachon *et al.* [2010] noted that floating chambers (of a different design) overestimate k_{600} by up to a factor 2 due to the chamber disturbing the water directly beneath and around it. However, the floating chambers of the design used in this study have been shown to yield k_{600} values that compare well to other non-invasive methods to estimate k_{600}, including existing wind speed-based models (see e.g. Gålfalk *et al.*, 2013; Schilder *et al.*, 2013), as opposed to the results presented by Vachon *et al.* [2010]. The k_{600} values we present here (Figure 2) are also in the same order of magnitude as k_{600} values predicted by the most often used wind speed models. Therefore, our results were apparently not significantly affected by a bias caused by chamber-induced turbulence effects.

Statistically significant correlations between U_{10} and k_{600} were apparent for all sampling stations except A1, which represented the most wind sheltered station (Pearson correlations, p from <0.05 to <0.0001, Table 2). The relationship between U_{10} and k_{600} varied between sampling stations (Figure 2, Table 2). Typically, the sites closest to the shore showed no (A1) or a weak (B1, C1) relationship whereas the more central sites had the strongest relationships, which is in agreement with the findings by *Schilder et al*. [2013] and *Vachon and Prairie* [2013]. It is important to note that these relationships are based on local k_{600} estimates but only one wind speed measurement location. Had wind speed been measured at each chamber location, more consistency among the relationships between U_{10} and k_{600} at the different

locations could be expected. We noted that most of the residual variability in Figure 2 was the result of 2 h chamber deployments, which suggests that the method is most robust if used for longer periods (6h or more). In support of this, *Gålfalk et al*. [2013] presented data showing large short-term (minutes-hours) variability of *k* at specific locations and distinct patches of surface water with different *k*-values were detected with Infra-Red imaging. A likely cause of this variability is variations in U_{10} at short time-scales and the lingering turbulence in the surface water. This can result in short-lived patches of surface water having different k_{600}-values than can be expected based on the current U_{10}.

3.3 Levels of C_{aq} and CH_4 fluxes from Lake Gerzensee

C_{aq} was highly variable between the different field campaigns, ranging from 0.04 mmol m^{-3} on 2 December 2013, to 7.0 mmol m^{-3} on 1-3 October 2012 and 56.0 mmol m^{-3} on 14 November 2013 (Figure 3; Table 3). Consequently, whole-lake *F* (based on C_{aq} and U_{10}-derived whole-lake *k*, see section 2.5) was also variable, and as low as 0.01 mmol m^{-2} day^{-1} on 2 December 2013, and as high as 15.9 mmol m^{-2} day^{-1} during lake overturning on 14 November 2013 (Figure 3; Table 3). The total open water CH_4 flux estimates (*F* + *E*), available for the first 6 lake visits (between October 2012 and September 2013), ranged from 1.1 mmol m^{-2} day^{-1} on 26-28 March 2013 to 13.9 mmol m^{-2} day^{-1} on 1-3 October 2012 (Figure 3; Table 3). *E* contributed 75 to 99 ‰ to the total CH_4 flux (on average 89 %).

High values during lake overturning in fall were observed for both *F* (2012 and 2013) and total CH_4 flux (2012). They are comparable to those reported by *Schubert et al*. [2012] in the period 27 October to 16 December 2008 in Lake Rotsee, another wind-shielded Swiss lowland lake. These authors found average whole-lake CH_4 flux (*F* + *E*) values of ~5 mmol m^{-2} day^{-1}, with peak emission events considerably higher (25 to 75 mmol m^{-2} day^{-1}). Due to our lower temporal sampling resolution, it is likely we missed such peak emission events at

Lake Gerzensee. However, the *F* estimate of 15.9 mmol m^{-2} day^{-1} on 14 November 2013 may have been such a peak emission event. *E* was not measured that date, but since *E* in our dataset ranged from 1.1 to 12.2 mmol m^{-2} day^{-1}, with the highest values in fall, total CH_4 emission from Lake Gerzensee may have been as high as 17.0 to 28.1 mmol m^{-2} day^{-1} on 14 November 2013.

To estimate mean open water CH_4 flux for the entire annual cycle we interpolated total open water CH_4 flux measurements between 1-3 October 2012 and 23-25 September 2013. Interpolated daily flux estimates then allowed the calculation of average CH_4 flux over the entire year. If we assume total ice cover on the lake and no CH_4 flux between 29 November 2012 and 25 March 2013, this results in a mean flux value across the year of 3.6 mmol m^{-2} day^{-1} for Lake Gerzensee. Since ice cover was probably not complete during this period and CH_4 may still have been produced and emitted after ice melt this estimate is likely conservative. If we allow the winter months to be included in the interpolation, the estimated annual CH_4 flux from Lake Gerzensee is equivalent to 5.8 mmol m^{-2} day^{-1}. For comparison with other lakes at different latitudes, the range of mean total CH_4 flux values reported for South American tropical and subtropical lakes and flood plains, measured in various seasons, is 1.5 to 13.5 mmol m^{-2} day^{-1} [*Bartlett et al*., 1988; *Devol et al.*, 1990; *Smith et al*., 2000; *Marani and Alvalá*, 2007; *Bastviken et al*., 2010]. Emissions in boreal lakes range from 0.06 to 2.7 mmol m^{-2} day^{-1}, respectively [*Bastviken et al*. 2011], and annual estimates for arctic thermokarst lakes range from 2.1 to 5.5 mmol m^{-2} day^{-1} [*Wik et al.*, 2016].

3.4 Spatial heterogeneity in C_{aq}, k and E

C_{aq} was not homogeneous within the lake during the first 6 visits: Single measurements ranged from 69 to 164 ‰ of whole-lake C_{aq} (standard deviation of ± 14 %; n = 300). *Hofmann* [2013] and *Schilder et al*. [2013] reported relatively lower C_{aq} in the lake centre than closer to the shore. In our study we found that the average of C_{aq} values at the central stations (A-C3 and D1) was similar to the average of C_{aq} values at localities closest to the shore (A-C1 and A-C2) (paired t-test, t 0.8394, $p>0.05$). However, the ratio between C_{aq} in the lake centre (stations A3, B3, C3, D) and C_{aq} close to the shore (stations A1, A2, B1, B2, C1, C2) at the beginning of day two and day three of each lake visit was significantly related with average U_{10} during the 24 h prior to sampling (Pearson correlation r -0.70, $p<0.05$, least square regression: $C_{aq(\text{Centre})}/C_{aq(\text{Shore})} = -0.16 \cdot U_{10} + 1.06$). With higher wind speed during the past 24 h period, surface water in the centre of the lake had relatively lower C_{aq}. This suggests that the C_{aq} patterns are modulated by wind and k, with higher k-values and, consequently, faster depletion of the dissolved CH_4 pool at the central sites. This suggests that at U_{10} values higher than we encountered (>3 m s^{-1}), spatial patterns in C_{aq} may need to be accounted for when sampling for C_{aq}. At low U_{10}, however, C_{aq} at the lake centre, station D, was not significantly different from whole-lake C_{aq} (paired t-test, t 1.208, $p>0.05$; n = 30). Altogether this points towards a situation where the spatial heterogeneity in C_{aq} may primarily be regulated by spatial heterogeneity on the export side (F), which interacts with short term temporal variability in wind speed.

Schilder et al. [2013] suggest that the relationship between U_{10} and k_{600} varies spatially due to changes in proximity to shore, height of sheltering structures along the shoreline, and general shape of the lake. This implies that, for a certain wind direction, repeated measurements along spatial transects on the same lake, in combination with one U_{10} estimate for the whole lake, should yield spatially variable relationships between k_{600} and U_{10} at the different sampling sites. Our data confirm this (Figure 2). Also, a transect from the centre of the lake to the upwind side of the lake should show a different spatial pattern in k_{600} than one from the centre to the downwind side, with higher k_{600} values on the downwind side due to the longer fetch. We found such an asymmetric distribution of the strength of the relationship between U_{10} and k_{600} (Figure 4). As suggested by *Schilder et al*. [2013] and *Vachon and Prairie* [2013], the strength of this relationship apparently depends on the fetch. However, it also appears to depend on the proximity to the shoreline, since it tends to become weaker in areas closer to the shore on both the upwind and downwind side of the lake, as suggested by *Schilder et al*. [2013].

Strong spatial patterns in *E* have been reported for temperate lakes in North America [*Bastviken et al*., 2004], Europe [*Hofmann et al*., 2010] and subtropical lakes and flood plains in South America [*Peixoto et al*., 2015]. These studies show that both the probability of *E* entering a floating chamber and the amount of CH_4 entering a floating chamber is clearly higher in shallower parts of the lakes close to the shore and emergent vegetation than in the lake centre. Likewise, higher densities of gas bubbles trapped in the ice covering an arctic lake were observed close to the shore [*Wik et al*., 2011], and the amount of CH_4 trapped in ice retrieved from arctic lakes was also higher in near-shore ice [*Phelps et al*., 1998]. Availability of organic matter in the sediments, wind-induced waves, and hydrostatic pressure changes have been identified as important determinants of *E* magnitude [*Keller and Stallard*, 1994; *Mattson and*

Likens, 1990; *Hofmann et al*., 2010; *Wik et al*., 2011]. Interestingly, *E* from Lake Gerzensee was distinctly higher in the central parts of the lake, with exception of 3 high *E* episodes at station C1 (Figure 5). This may be related to the low wind speeds typical for the lake, steep slopes of Lake Gerzensee facilitating sediment focusing to deeper regions (Figure 1c), very small area of shallow water (<2 m water depth), a relatively higher proportion of easily degradable organic matter (e.g. algae) in central sediments than in the near-shore zone and the strong seasonal stratification of the lake which results in anoxic waters below ~6 m water depth between June and October.

3.5 Comparing the locally calibrated U_{10}-k_{600} relationship to existing general models

We used our site-specific linear U_{10}-k_{600} relationships (Figure 2) to construct a locally calibrated whole-lake relationship between k_{600} and U_{10} (Figure 6a). Whole-lake k_{600} is calculated as the average of k_{600} values of all sampling stations at a given value of U_{10}, as predicted by the relationships between U_{10} and k_{600} for the individual sampling sites (Figure 2, Table 2), weighted by the proportion of lake area each sampling station represents. For 8 of the 19 sampling intervals used for determining site-specific relationships between k_{600} and U_{10} we obtained k_{600} values at all the sampling stations. For these sampling intervals whole lake estimates of k_{600} values calculated as the mean values measured at the different sampling stations, weighted by the lake area they represent, were in close agreement with the whole-lake relationship derived from the site-specific relationships (Figure 6a). The residuals (modeled – observed) range from -0.27 to 0.53 cm h^{-1} (average 0.08 ± 0.24 cm h^{-1}). Our lake-specific relationship predicts whole-lake k_{600} values that are in the range of those produced by existing general models by *Liss and Merlivat* [1986], *Cole and Caraco* [1998], and *Crusius and Wanninkhof* [2003] (Figure 6b). It suggests a linear relationship within the U_{10} range of 0-3 m s^{-1}, in agreement with general models presented by *Crusius and Wanninkhof* [2003]

(models A and C in their Figure 3) and *Liss and Merlivat* [1986] (Figure 6b). The slope of our site-specific relationship resembled one of the models presented by *Crusius and Wanninkhof* [2003] (model A in their Figure 3), and was much steeper than suggested by *Crusius and Wanninkhof* [2003] (model C in their Figure 3) and *Liss and Merlivat* [1986]. The intercept, in turn, agreed with the intercept given by *Crusius and Wanninkhof* [2003] (model C in their Figure 3). The predicted k_{600} values, however, lie in general closest to the model by *Cole and Caraco* [1998], who suggested a non-linear relationship between the two variables. U_{10} in SF_6 tracer studies is usually measured in the centre of the lake [e.g. *Cole and Caraco*, 1998; *Crusius and Wanninkhof*, 2003] and we measured wind speed at the shoreline. Possibly our U_{10} values would have been slightly higher had we measured in the lake centre, accounting for some of the discrepancy. The same relationship calculated for Lake Gerzensee based on the 18 h measurements only (from late afternoon until the next morning) yields whole lake k_{600} values 16 % higher than the one based solely on 6 h measurements (ca 10.00 to 16.00 h) at U_{10} of 0.1 m s^{-1}, and 5 % higher at a U_{10} of 2.7 m s^{-1}, and this difference declines further with increasing U_{10}. This may be due to the effects of buoyancy flux [*MacIntyre et al*., 2001] as lake water cools at the surface during the night and mixing of surface water layers enhances the gas exchange rates. *Gålfalk et al*. [2013] show how chambers of our specific design are able to register this convective component of *k*.

There are considerable differences in k_{600} and, consequently, *F* estimates predicted by our locally calibrated relationship compared with existing general models for inferring *F* from

U_{10}-derived k-values (Figure 6c). Depending on U_{10} and the model of choice, the returned k values can be more than 200 % and less than 50 % of the locally calibrated values. As a consequence, resulting estimates of F may be under- or overestimated by a factor 2 if a general model is applied that is not calibrated to the local system. A locally calibrated relationship between k_{600} and U_{10} based on just one of the sampling sites we selected yields k_{600} values that amount to between 25 % (near-shore) and 150 % (lake centre) of the spatially resolved relationship we obtained, which could lead to under- and overestimates of F of similar magnitude (and possibly larger overestimations at higher wind speeds). Because strong spatial patterns in both F and E have been reported in multiple studies [e.g. Schilder et al., 2013; Vachon and Prairie 2013; Peixoto et al., 2015], there is considerable room for improvement of global freshwater greenhouse gas emission estimates if spatial variability is taken into account. Constructing spatially resolved lake-specific relationships between k_{600} and U_{10} may therefore significantly improve the accuracy of such inferences and should be considered in studies that monitor individual lakes for a longer period of time. After the first visit to the lake (October 2012), when primarily very low wind speeds were recorded (0.1 to 0.9 m s^{-1}), the resulting whole-lake relationship between k_{600} and U_{10} differed from the relationship we established after four visits, especially for higher values of U_{10} (Figure 6d). However, after the second visit (26-28 November 2012), with U_{10} values ranging from 0.3 to 2.7 m s^{-1}, the data from both visits combined already yielded a relationship very similar to the one we derived after four visits (Figure 6d). This suggests that a robust locally calibrated relationship between U_{10} and k_{600} may be obtained based on only a few visits, provided the wind conditions encountered encompass the range of wind speeds that is expected on the lake system of interest.

For studies that visit a lake only once, *Vachon and Prairie* [2013] propose several ways of correcting for system specific characteristics, including a lake size correction. Their proposed model for a lake the size of Lake Gerzensee (0.24 km^2) returned k_{600} values higher than we observed, however, while it performs very well within their data set. Their intercept (U_{10} = 0) of 2.51 cm h^{-1} (95% confidence interval ± 0.99 cm h^{-1}) is higher than in our relationship (0.90 cm h^{-1}). The slope (1.23) in the model by *Vachon and Prairie* [2013] is also higher than we inferred (0.97), but our slope lies within their 95 % confidence interval (Figure 5 in *Vachon and Prairie* [2013]). Both studies seem to agree on the strength of the interaction between U_{10} and *k* (i.e. the slope), but differ in terms of *k*-values in (near) absence of wind. While *Vachon and Prairie* [2013] also used floating chambers to infer k_{600}, there are some differences in the approach used compared to in our study. For example, *Vachon and Prairie* [2013] measured for 1 minute intervals during 10 minutes, and used CO_2 accumulation to infer *k* [*Vachon et al*., 2010], whereas we used longer deployments and CH_4 accumulation. *Vachon and Prairie* [2013] also reduced their inferred *k*-values to correct for turbulence caused by the chamber. We did not do this as the type of chamber used has been confirmed to not bias fluxes compared to other methods [e.g. *Gålfalk et al*., 2013]. One concern recently raised with gas fluxes from lakes is the suggestion that microbubbles can cause overestimated *k* values [*McGinnis et al*., 2015]. However, because our k_{600} values were low given the literature range and lower than those estimated from the CO_2-based model of *Vachon and Prairie* [2013] there were no signs of microbubbles in our study.

5 Conclusions

Since k is an important driver of not only F of CH_4 but also F of other greenhouse gas such as CO_2 and N_2O, our study demonstrates that there can be a substantial spatial variability in greenhouse gas emissions from lakes, and that emission estimates based on U_{10}-derived k can be substantially improved by limited, but carefully designed empirical measurements of k and U_{10} at the study sites of interest. Importantly, this can easily be done in systems where long data series already exist. We have also shown strong temporal variability in CH_4 emissions from Lake Gerzensee, with emissions one order of magnitude higher in fall than in spring. These strong spatio-temporal patterns in greenhouse gas flux magnitude need to be accounted for when upscaling short-term and single-spot measurements to whole-lake, whole-year estimates. Our findings highlight the need for more measurements of lacustrine greenhouse gas flux that are spatially resolved and cover long time periods. Such studies would provide valuable information for future efforts to better quantify the contributions of lakes to the continental greenhouse gas budget.

Acknowledgments

We thank Clemens Stampfli, Studienzentrum Gerzensee and the Stiftung der Schweizerischen Nationalbank for providing access to Lake Gerzensee, the boathouse and their boats, and we thank Marina Morlock and Tabea Stötter for assistance during part of the field work, and Päivi Rinta for creating the lake maps. We thank Meteo Swiss for providing wind speed data for one of our visits. We also thank two anonymous reviewers for their constructive comments. This research was supported by the European Research Council (ERC) under the European Union's Seventh Framework Programme (FP/2007-2013)/ERC Grant Agreement n. 239858 and by the Swedish Research Council (VR). The data used in this manuscript can be found in Supplementary Table 1.

References

Bade, D. L. (2009), Gas exchange at the air-water interface, in *Encyclopedia of Inland Waters*, edited by G. E. Likens, pp. 70–78, Elsevier, Oxford.

Bartlett, K. B., P. M. Crill, D. I. Sebacher, R. C. Harriss, J. O. Wilson, and J. M. Melack (1988), Methane flux from the central Amazonian floodplain, *J. Geophys. Res.*, *93*, 1571–1582, doi:10.1029/JD093iD02p01571.

Bastviken, D., J. Cole, M. Pace, and L. Tranvik (2004), Methane emissions from lakes: Dependence of lake characteristics, two regional assessments, and a global estimate, *Global Biogeochem. Cycles*, *18*(4), GB4009, doi:10.1029/2004GB002238.

Bastviken, D., A. L. Santoro, H. Marotta, Q. Pinho, D. F. Calheiros, P. Crill, and A. Enrich-Prast (2010), Methane emissions from Pantanal, South America, during the low water season: Toward more comprehensive sampling, *Environ. Sci. Technol.*, *44*, 5450–5455.

Bastviken, D., L. J. Tranvik, J. A. Downing, P. M. Crill, and A. Enrich-prast (2011), Freshwater methane emissions offset the continental carbon sink, *Science*, *331*, 50, doi:10.1126/science.1196808.

Battin, T. J., S. Luyssaert, L. A. Kaplan, A. K. Aufdenkampe, A. Richter, and L. J. Tranvik (2009), The boundless carbon cycle, *Nat. Geosci.*, *2*(9), 598–600, doi:10.1038/ngeo618.

Cole, J. I., and N. F. Caraco (1998), Atmospheric exchange of carbon dioxide in a low-wind oligotrophic lake measured by the addition of SF_6, *Limnol. Oceanogr.*, *43*(4), 647–656.

Cole, J. J. et al. (2007), Plumbing the global carbon cycle: integrating inland waters into the terrestrial carbon budget, *Ecosystems*, *10*(1), 172–185, doi:10.1007/s10021-006-9013-8.

Cole, J. J., D. L. Bade, D. Bastviken, M. L. Pace, and M. Van De Bogert (2010), Multiple approaches to estimating air-water gas exchange in small lakes, *Limnol. Oceanogr. Methods*, *8*, 285–293.

Crusius, J., and R. Wanninkhof (2003), Gas transfer velocities measured at low wind speed over a lake, *Limnol. Oceanogr.*, *48*(3), 1010–1017, doi:10.4319/lo.2003.48.3.1010.

Devol, A. H., J. E. Richey, W. A. Clark, and S. L. King (1988), Methane emissions to the troposphere from the Amazon floodplain, *J. Geophys. Res.*, *93*, 1583–1592.

Downing, J. A., and C. M. Duarte (2009), Lakes (Formation, diversity, distribution), in *Encyclopedia of Inland Waters*, edited by G. E. Likens, pp. 469–478, Elsevier, Oxford.

Gålfalk, M., D. Bastviken, S. Fredriksson, and L. Arneborg (2013), Determination of the piston velocity for water-air interfaces using flux chambers, acoustic Doppler velocimetry,

and IR imaging of the water surface, *J. Geophys. Res. Biogeosciences*, *118*(2), 770–782, doi:10.1002/jgrg.20064.

Hammer, Ø., D. A. T. Harper, and P. D. Ryan (2001), PAST: paleontological Statistics software package for education and data analysis, *Paleontol. Electron.*, *4*(1), 9.

Hofmann, H. (2013), Spatiotemporal distribution patterns of dissolved methane in lakes: How accurate are the current estimations of the diffusive flux path?, *Geophys. Res. Lett.*, *40*(11), 2779–2784, doi:10.1002/grl.50453.

Hofmann, H., L. Federwisch, and F. Peeters (2010), Wave-induced release of methane: Littoral zones as a source of methane in lakes, *Limnol. Oceanogr.*, *55*(5), 1990–2000, doi:10.4319/lo.2010.55.5.1990.

Keller, M., and R. F. Stallard (1994), Methane emission by bubbling from Gatun Lake, Panama, *J. Geophys. Res.*, *99*, 8307–8319.

Liss, P. S., and L. Merlivat (1986), Air-sea gas exchange rates: Introduction and synthesis, in *The role of air-sea exchange in geochemical cycling*, edited by P. E. Buat-Menard, pp. 113–127, D. Reidel, Dordrecht.

Macintyre, S., W. Eugster, and G. W. Kling (2001), The critical importance of buoyancy flux for gas flux across the air-water interface, in *Gas transfer at water surfaces*, edited by M. A. Donelan, W. M. Drennan, E. S. Saltzman, and R. Wanninkhof, pp. 135–139, AGU, Washington.

Marani, L., and P. C. Alvalá (2007), Methane emissions from lakes and floodplains in Pantanal, Brazil, *Atmos. Environ.*, *41*(8), 1627–1633, doi:10.1016/j.atmosenv.2006.10.046.

Mattson, M. D., and G. E. Likens (1990), Air pressure and methane fluxes, *Nature*, *347*, 718–719.

McGinnis, D. F., G. Kirillin, K. W. Tang, S. Flury, P. Bodmer, C. Engelhardt, P. Casper, and H.-P. Grossart (2015), Enhancing surface methane fluxes from an oligotrophic lake: exploring the microbubble hypothesis., *Environ. Sci. Technol.*, *49*(2), 873–80, doi:10.1021/es503385d.

Miettinen, H., J. Pumpanen, J. J. Heiskanen, H. Aaltonen, I. Mammarella, A. Ojala, J. Levula and M. Rantakari (2015), Towards a more comprehensive understanding of lacustrine greenhouse gas dynamics - Two-year measurements of concentrations and fluxes of CO_2, CH_4 and N_2O in a typical boreal lake surrounded by managed forests., *Boreal Env. Res.*, *20*, 75–89.

Myhre, G. et al. (2013), Anthropogenic and Natural Radiative Forcing, in *Climate Change 2013: The Physical Science Basis. Contribution of Working Group I to the Fifth Assessment Report of the Intergovernmental Panel on Climate Change*, edited by T. F. Stocker, D. Qin, G.-K. Plattner, M. Tignor, S.-K. Allen, J. Boschung, A. Nauels, Y. Xia, V. Bex, and P. M. Midgley, pp. 659–740, Cambridge, United Kingdom and New York, NY, USA.

Peixoto, R. B., F. Machado-Silva, H. Marotta, A. Enrich-Prast, and D. Bastviken (2015), Spatial versus day-to-day within-lake variability in tropical floodplain lake CH4 emissions--developing optimized approaches to representative flux measurements., *PLoS One*, *10*(4), e0123319, doi:10.1371/journal.pone.0123319.

Phelps, A. R., K. M. Peterson, and M. O. Jeffries (1998), Methane efflux from high-latitude lakes during spring ice melt, *J. Geophys. Res.*, *103*, 29029–29036.

Read, J. S. et al. (2012), Lake-size dependency of wind shear and convection as controls on gas exchange, *Geophys. Res. Lett.*, *39*(9), L09405, doi:10.1029/2012GL051886.

Rinta, P., D. Bastviken, M. van Hardenbroek, P. Kankaala, M. Leuenberger, J. Schilder, T. Stötter, and O. Heiri (2015), An inter-regional assessment of concentrations and $\delta^{13}C$ values of methane and dissolved inorganic carbon in small European lakes, *Aquat. Sci.*, *77*(4), 667–680, doi:10.1007/s00027-015-0410-y.

Schilder, J., D. Bastviken, M. van Hardenbroek, P. Kankaala, P. Rinta, T. Stötter, and O. Heiri (2013), Spatial heterogeneity and lake morphology affect diffusive greenhouse gas emission estimates of lakes, *Geophys. Res. Lett.*, *40*(21), 5752–5756, doi:10.1002/2013GL057669.

Schubert, C. J., T. Diem, and W. Eugster (2012), Methane emissions from a small wind shielded lake determined by eddy covariance, flux chambers, anchored funnels, and boundary model calculations: a comparison., *Environ. Sci. Technol.*, *46*(8), 4515–22, doi:10.1021/es203465x.

Smith, L. K., W. M. Lewis, J. P. Chanton, G. Cronin, and S. K. Hamilton (2000), Methane emissions from the Orinoco River floodplain, Venezuela, *Biogeochemistry*, *51*, 113–140.

Tranvik, L. J. et al. (2009), Lakes and reservoirs as regulators of carbon cycling and climate, *Limnol. Oceanogr.*, *54*(1), 2298–2314.

Vachon, D., and Y. T. Prairie (2013), The ecosystem size and shape dependence of gas transfer velocity versus wind speed relationships in lakes, *Can. J. Fish. Aquat. Sci.*, *70*(August), 1757–1764, doi:10.1139/cfjas-2013-0241.

Vachon, D., Y. T. Prairie, and J. J. Cole (2010), The relationship between near-surface turbulence and gas transfer velocity in freshwater systems and its implications for floating chamber measurements of gas exchange, *Limnol. Oceanogr.*, *55*(4), 1723–1732, doi:10.4319/lo.2010.55.4.1723.

Wik, M., P. M. Crill, D. Bastviken, Å. Danielsson, and E. Norbäck (2011), Bubbles trapped in arctic lake ice: Potential implications for methane emissions, *J. Geophys. Res.*, *116*, G03044, doi:10.1029/2011JG001761.

Wik, M., B. F. Thornton, D. Bastviken, J. Uhlbäck, and P. M. Crill (2016), Biased sampling of methane release from northern lakes: a problem for extrapolation, *Geophys. Res. Lett.*, *43*, 1256–1262, doi:0.1002/2015GL066501.

Wik, M., Varner, R. K., Anthony, K. W., MacIntyre, S., & Bastviken, D. (2016). Climate-sensitive northern lakes and ponds are critical components of methane release. *Nature Geoscience*, *9*(2), 99–106. http://doi.org/10.1038/ngeo2578

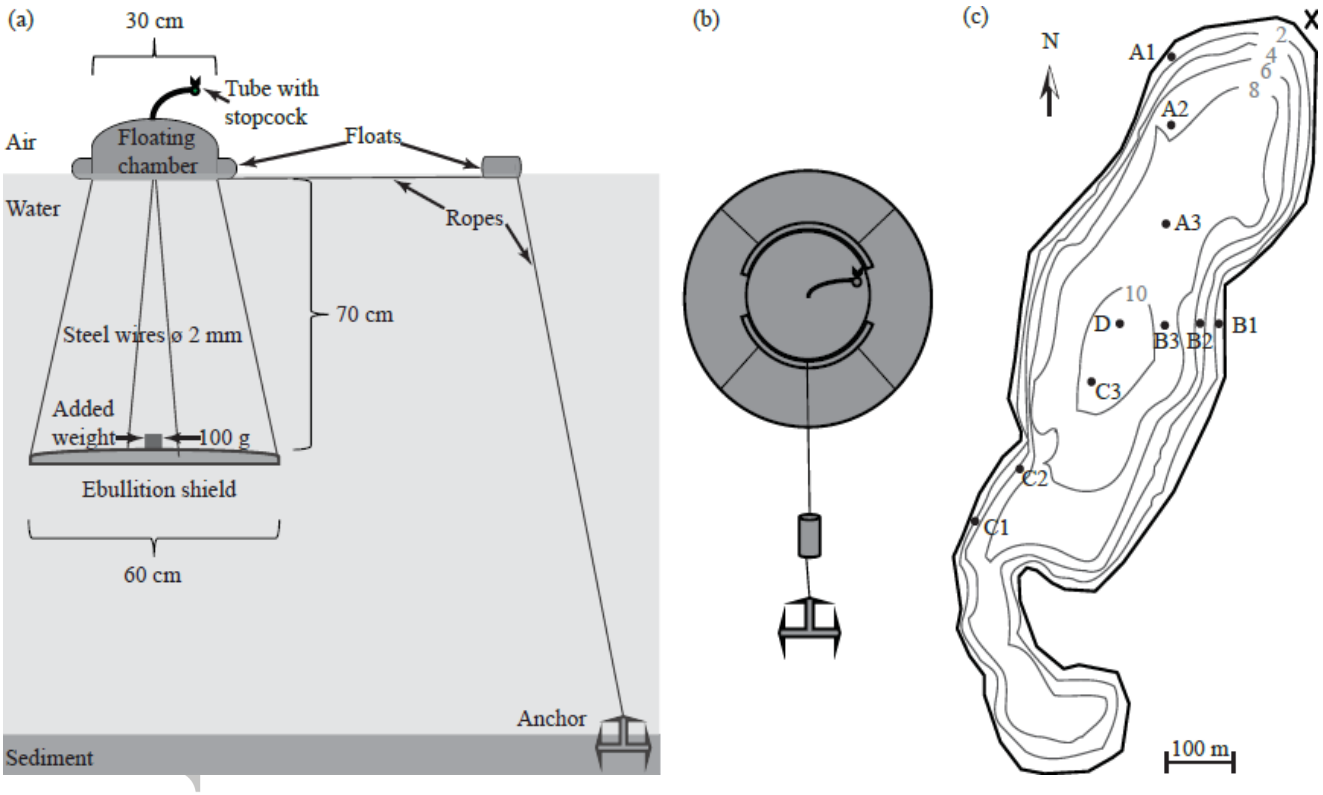

Figure 1: (a) Schematic representation of our adaptations to the floating chamber design presented by *Cole et al*. [2010]. (b) Top view of our shielded floating chamber setup. (c) Bathymetric map of Lake Gerzensee showing the locations of the sampling stations. The numbers indicate the depths of the isobaths, and the X marks the location of the weather station.

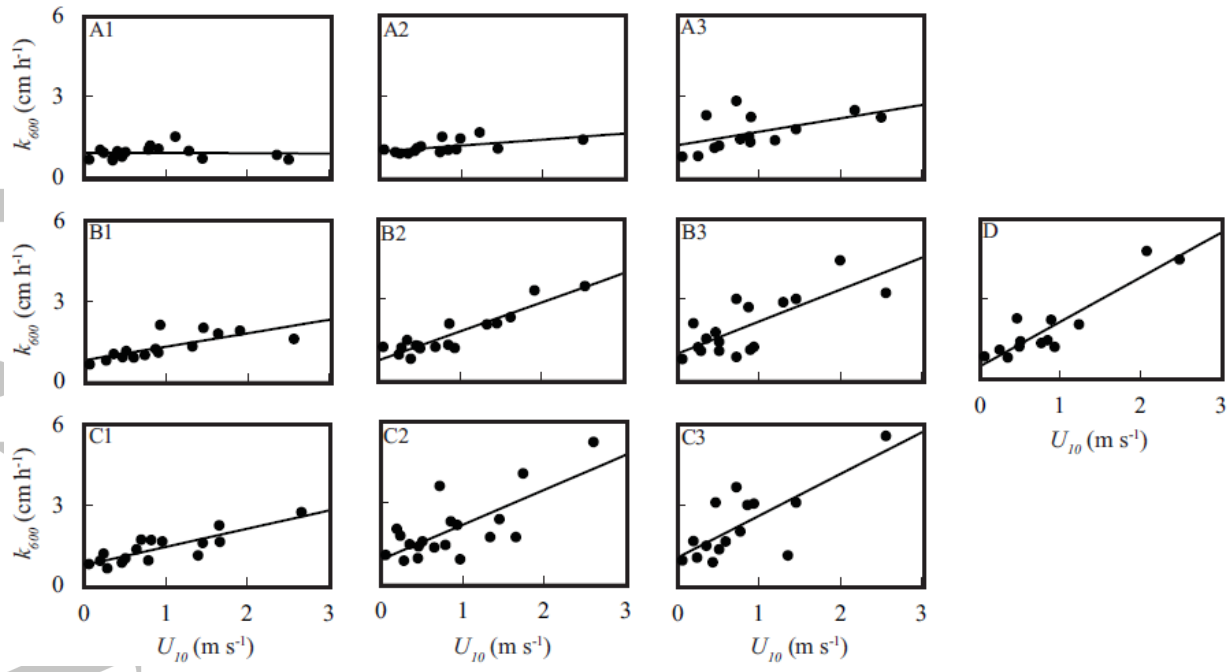

Figure 2: U_{10} versus k_{600} for each sampling station on Lake Gerzensee. The lines through the data points were fitted using linear least square regressions (Table 2).

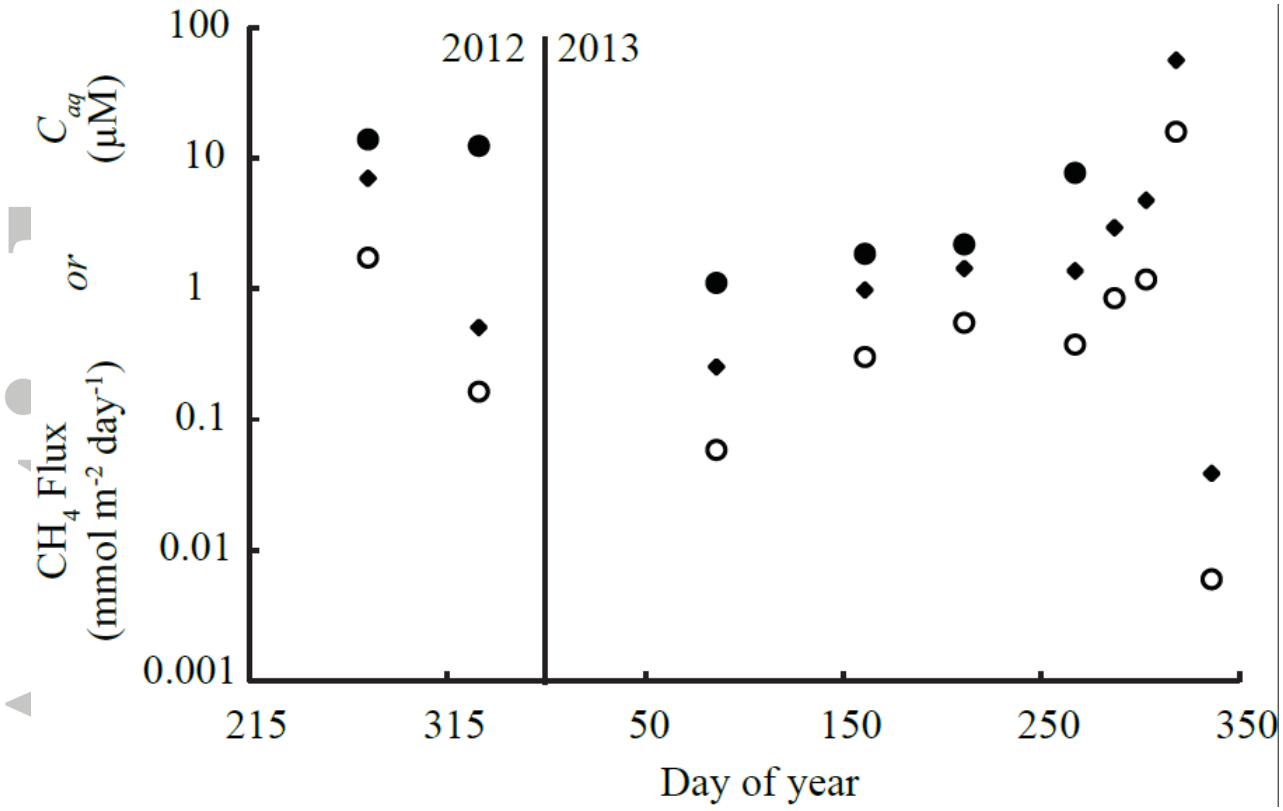

Figure 3: Surface water CH_4 concentrations and CH_4 emissions from Lake Gerzensee. Whole-lake F for Lake Gerzensee based on U_{10}, C_{aq} and the lake-specific relationship between k and U_{10} developed during this study (mmol m^{-2} day^{-1}) is indicated by open circles, C_{aq} (mmol m^{-3}) by closed diamonds and whole-lake total CH_4 flux (mmol m^{-2} day^{-1}) (including ebullition) estimated for the lake based on the first 6 lake visits by closed circles. Note the log scale on the y-axis.

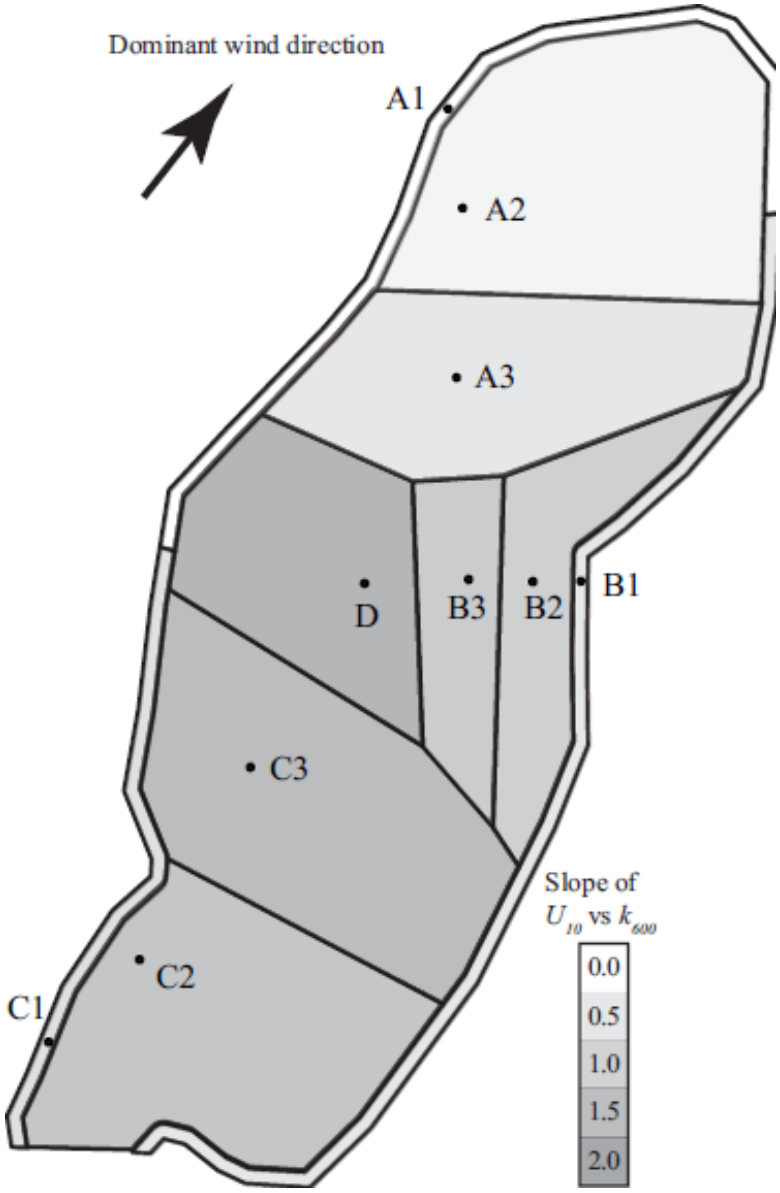

Figure 4: Map of Lake Gerzensee showing the sampling sites and the lake area they represent. The shading shows the slope of the relationship between U_{10} (m s^{-1}) and k_{600} (cm h^{-1}) for each sampling site (see Table 2).

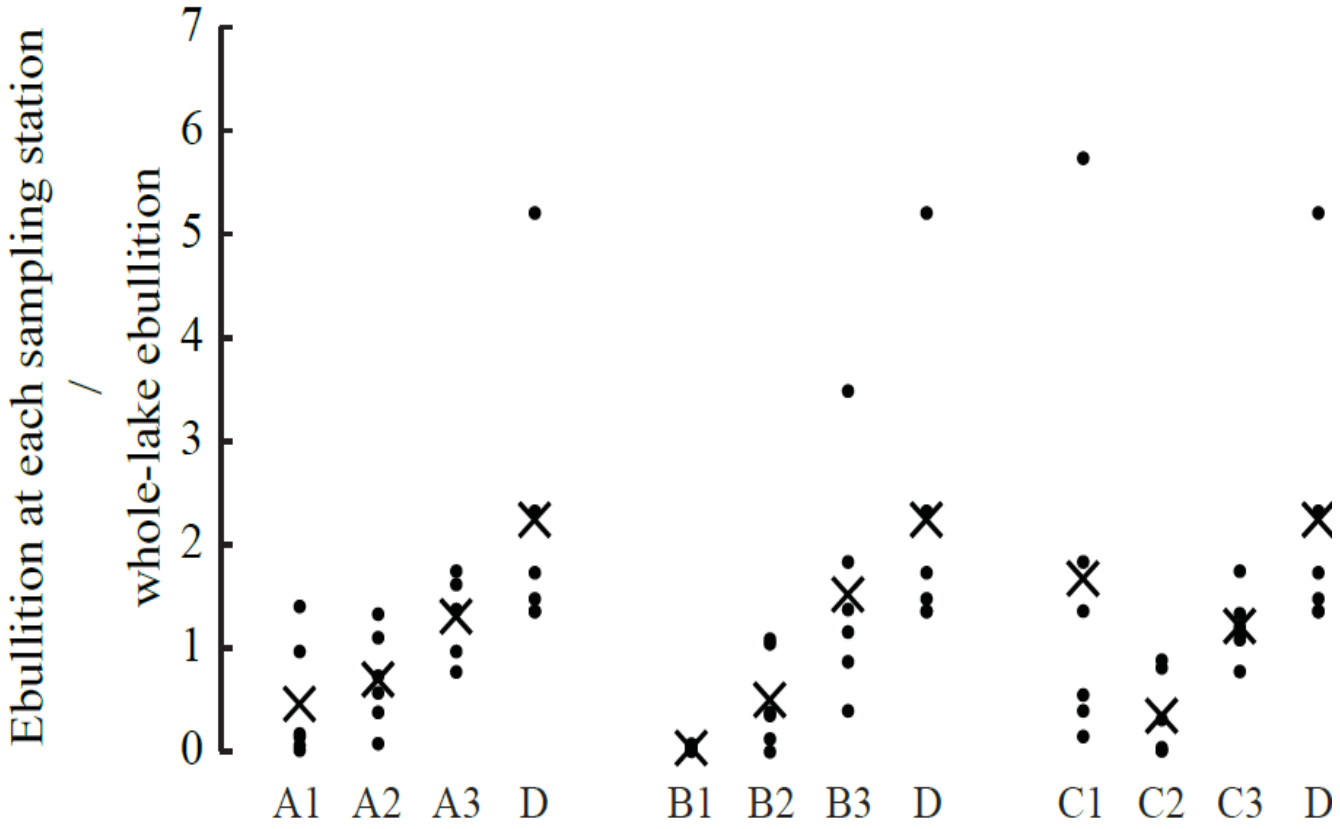

Figure 5: Ebullitive CH_4 flux for each site divided by whole-lake ebullitive CH_4 flux for the first 6 visits for which ebullition data are available. Dots represent individual measurements during the 6 visits, and the "X"-marks the average of the individual measurements.

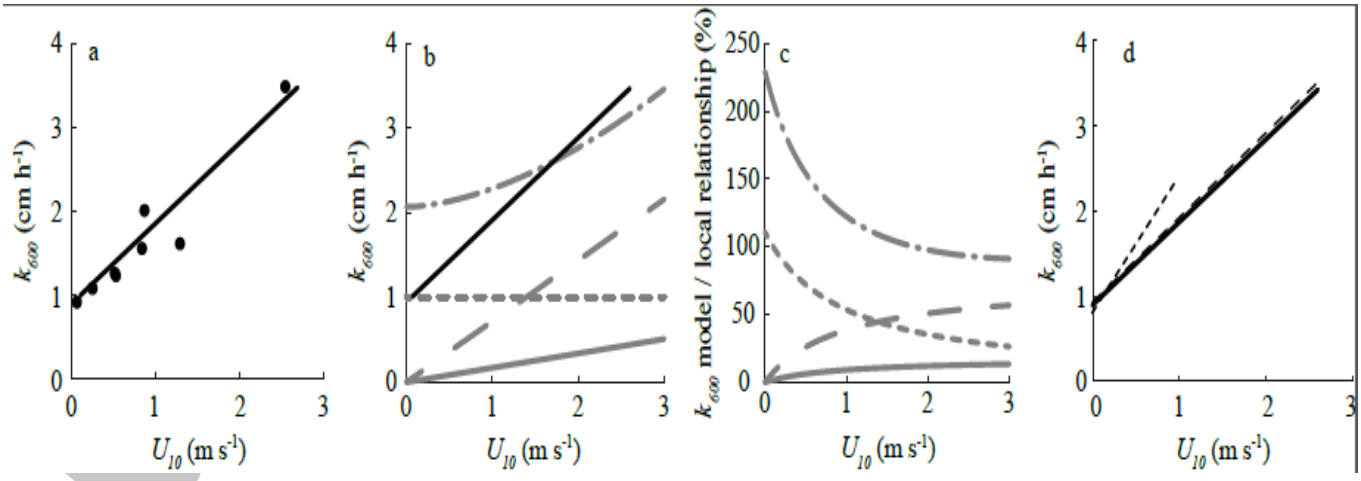

Figure 6: (a) Our whole-lake relationship between U_{10} and k_{600} (black line) based on the average of k_{600} values predicted at individual sampling stations at a given value of U_{10} (Figure 2), weighted by the proportion of lake area each sampling station represents (Figure 4). The model is compared with observed whole-lake k_{600} estimates based on the 8 measurement intervals that yielded k_{600} values for all sampling stations on the lake (black dots). (b) Our whole-lake relationship between U_{10} and k_{600} (black line) compared with existing general models (grey lines): *Liss and Merlivat* [1986, solid line], *Cole and Caraco* [1998, dash-dotted line], model A in Figure 3 in *Crusius and Wanninkhof* [2003, long dased line], and model C in their Figure 3: short dashed line. (c) The over- or underestimation (%) of whole-lake k_{600} by the existing general models compared to our lake-specific model (lines represent the same models as in panel b). (d) Whole-lake relationship between U_{10} and k_{600} for Lake Gerzensee calculated after the first lake visit (short dashed line), after the second visit (long dashed line), and after four visits, which is the model presented in panel a (solid line).

Table 1. Field campaign design.

Schematic overview of sampling and research tasks during the field campaign between October 2012 and December 2013. X indicates sampling for a specific research task on the sampling date.

	1-3 Oct 2012	26-28 Nov 2012	26-28 Mar 2013	10-12 Jun 2013	29-31 Jul 2013	23-25 Sep 2013	14 Oct 2013	30 Oct 2013	14 Nov 2013	2 Dec 2013
Spatially resolved k determinations to derive lake-specific relationship between k and U_{10}	X	X	X	X	-	-	-	-	-	-
Spatially resolved total CH_4 flux determination to estimate ebullitive CH_4 flux	X	X	X	X	X	X	-	-	-	-
F_{CH4} estimates based on whole-lake C_{aq} and U_{10}-derived k	X	X	X	X	X	X	-	-	-	-
F_{CH4} estimates based on C_{aq} in the lake centre and U_{10}-derived k	-	-	-	-	-	-	X	X	X	X

Table 2. Site-specific relationships between U_{10} and k_{600}.

The proportion of lake area (A) represented by each sampling station, slopes, intercepts and 95 % confidence intervals of the slopes and intercepts for the sampling station-specific linear least square regressions between U_{10} and k_{600} (k_{600} = Slope * U_{10} + Intercept), together with r and p values (Pearson correlations) for these relationships.

Chamber	A	Slope	95 % CI slope		Intercept	95 % CI intercept		r	p
A1	0.03	-0.01	-0.11	0.38	0.91	0.69	1.07	-0.03	0.91
A2	0.18	0.22	0.10	0.62	0.95	0.74	1.06	0.56	<0.05
A3	0.14	0.50	0.08	0.87	1.19	0.74	1.82	0.53	<0.05
B1	0.04	0.50	0.31	0.88	0.79	0.52	1.06	0.73	<0.005
B2	0.08	1.08	0.73	1.30	0.72	0.47	0.97	0.92	<0.0001
B3	0.05	1.19	0.72	1.84	0.98	0.42	1.42	0.75	<0.0005
C1	0.02	0.68	0.39	0.86	0.75	0.56	1.00	0.84	<0.0001
C2	0.16	1.30	0.27	1.74	0.89	0.41	1.58	0.73	<0.0005
C3	0.18	1.56	0.17	2.31	1.04	0.54	1.86	0.75	<0.005
D	0.11	1.68	0.71	2.12	0.44	-0.04	0.99	0.91	<0.0005

Table 3. Whole lake C_{aq} and CH_4 flux.

Sampling dates, whole-lake C_{aq} (µM; * indicates estimates based on C_{aq} at station D only), F (mmol m^{-2} day^{-1}), E (mmol m^{-2} day^{-1}), and total CH_4 flux (F+E, mmol m^{-2} day^{-1}) on these dates. The last column gives the proportion of total CH_4 flux originating from F. NA indicates E was not measured that date.

Date	C_{aq} (µM)	F_{CH4} (mmol m^{-2} day^{-1})	Ebullitive CH_4 flux (mmol m^{-2} day^{-1})	Total Flux (mmol m^{-2} day^{-1})	% F_{CH4} of total Flux
1-3 October 2012	7.00	1.73	12.18	13.91	12.43
26-28 November 2012	0.51	0.16	12.21	12.37	1.33
26-28 March 2013	0.25	0.06	1.05	1.11	5.27
10-12 June 2013	0.98	0.30	1.56	1.86	16.20
29-31 July 2013	1.44	0.55	1.64	2.19	25.21
23-25 September 2013	1.37	0.38	7.35	7.73	4.86
14 October 2013	2.94*	0.88	NA	NA	NA
30 October 2013	4.77*	1.18	NA	NA	NA
14 November 2013	56.04*	15.89	NA	NA	NA
2 December 2013	0.04*	0.01	NA	NA	NA